Optical Materials 149 (2024) 115122

Contents lists available at ScienceDirect

Optical Materials

journal homepage: www.elsevier.com/locate/optmat

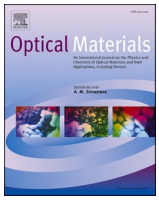

Research Article

Influence of shallow traps on the kinetics of Optically Stimulated Luminescence of the Li and Ce ions co-doped MgB_4O_7 compound

Adelmo S. Souza [a], Jorge L.O. Santos [a], Vinicius Coelho [a], Antonio O. de Souza [a], João V. B. Valença [b], Iury S. Silveira [c], Linda V.E. Caldas [c], Heveson Lima [d,*]

[a] Centro Multidisciplinar de Bom Jesus da Lapa, Universidade Federal do Oeste da Bahia, 47600-000, Bom Jesus da Lapa, BA, Brazil
[b] Grupo de Física Médica Experimental e Computacional, Departamento de Ciências Exatas e Sociais Aplicadas, Universidade Federal de Ciências da Saúde de Porto Alegre, 40050-170, Porto Alegre, RS, Brazil
[c] Instituto de Pesquisas Energéticas e Nucleares, Comissão Nacional de Energia Nuclear, 05508-000, São Paulo, SP, Brazil
[d] Centro Multidisciplinar de Luís Eduardo Magalhães, Universidade Federal do Oeste da Bahia, 47855-218, Luís Eduardo Magalhães, BA, Brazil

ARTICLE INFO

Keywords:
Shallow traps
Rate law
Photoionization cross-section
Optically stimulated luminescence
Thermoluminescence

ABSTRACT

The presence of point defects associated with shallow traps has been identified as a limiting factor in the design of materials with desirable characteristics for applications such as scintillation and luminescence dosimetry, among others. In this context, this study aims to elucidate the dynamics inherent to the charge carriers in systems containing multiple traps and one single recombination centre. To unravel this complexity, we employed a synergetic approach combining Thermoluminescence (TL) and Optically Stimulated Luminescence (OSL) measurements with kinetic models. Specifically, for the Li and Ce co-doped MgB_4O_7, we verified that the electron population trapped in shallower traps exhibits a slower decay rate under optical stimulation compared to deeper traps. This behaviour led to a delay in the luminescence emission, as a result of charge re-trapping or even competition with other centres. This phenomenon can be attributed to its low photoionization cross-section associated with a high re-trapping rate, providing a rationale for these remarks. In addition, we observed that the shallow traps have a greater optical than thermal probability of being detrapped, indicating that they were not solely detrapped through thermal stimulation. Also, the magnitude of the thermal probability leads us to believe that there is an electron population different from zero in the conduction band at $t = 0$ (before optical stimulation). Lastly, this study paves the way for a deeper understanding of charge carrier dynamics in systems of multiple traps, improving the performance of existing materials for scintillation and dosimetry.

1. Introduction

There is a substantial interest in the phenomenon of optically stimulated luminescence (OSL) due to applications such as radiation dosimetry [1–3], medical imaging [4,5], nanothermometry [6,7], among others. These applications are based on the assumption that electrons become trapped in metastable states within the materials bandgap as a result of previous exposure to ionising radiation. When the material is optically stimulated, these trapped electrons are released into the conduction band. Subsequently, they recombine with holes at the recombination centres, potentially leading to the emission of light. The intensity of the luminescent signal is employed to estimate the absorbed dose (usually measured in Gy) that the material was exposed to due to ionising radiation. The materials assessed for their potential as radiation detectors to perform the quoted estimation (often referred to as 'dosimeters') should preferentially exhibit specific characteristics, such as: a linear dose-response for a broad dose range, high sensitivity, measurement reproducibility, and signal stability over time [8,9]. Usually the materials contain more than one set of electron traps – density of discrete electron traps per unit volume at a specific depth – which leads to the evidence of competing processes with regards to the recombination probability [10,11]. Commonly, theoretical approaches assume that in an OSL experiment, electrons are solely released through optical stimulation. However, this assumption is not valid in the presence of shallow traps. In such cases, the thermal energy associated with the ambient temperature is sufficient to release the electrons that are localized in the shallow traps [12]. Consequently, in this situation, both thermal and optical stimulation occur simultaneously in an

* Corresponding author.
E-mail addresses: heveson.matos@ufob.edu.br, heveson@hotmail.com (H. Lima).

https://doi.org/10.1016/j.optmat.2024.115122
Received 15 December 2023; Received in revised form 10 February 2024; Accepted 18 February 2024
Available online 28 February 2024

experimental OSL analysis. While the impact of shallow traps has been previously examined by different groups [13], the intricate nature of the phenomenon gives rise to experimental constraints when attempting to elucidate the true role of these traps.

There are numerous effects attributed to shallow traps [12,13]. Materials harbouring shallow traps exhibit a gradual decline with increasing delay in TL measurements, a phenomenon known as fading. This effect is understood as the release of electrons from shallow trap levels through, for example, thermally activated processes at room temperature [14]. Yukihara et al. proposed that shallow traps are associated with the fast OSL components in the initial part of the OSL decay curve [15]. However, the non-linear dose dependence of the signal, quenching of luminescence, anomalous fading [9], and an increase in lifetime [13] can also result from a simple model involving empty trapping states [16]. Indeed, only under simplifying assumptions does the competition between recombination centres and empty traps result in a linear effect. Determining the contribution of each trap to the OSL signal is a fundamental question for understanding the kinetics of the phenomenon. Therefore, experimental studies investigating changes in trapped electron concentrations within each trap during OSL measurements are crucial for theoretical models.

The concentration of trapped electrons before and after an OSL measurement was presented by Jain et al. [17] using a coupled radio-photoluminescence/OSL system. However, this was applied in a feldspar system that presents solely one set of traps. Thermoluminescence (TL) is ideal for probing the trap depths in materials, as the signal is composed of emissions that can be present in only one or more temperature intervals, depending on the distribution of trap levels presented in the sample. Changes in the relative intensity of the TL glow peaks allow us to experimentally extract information on the competition between the recombination centre and empty traps [18].

In this context, the main goal of the present work is to contribute to the discussion on the dynamic processes in a system with multiple sets of electron traps and one recombination centre. For this, we combined TL and OSL measurements, coupled with kinetic models, to analyse the charge carrier dynamics. An additional term of temperature was incorporated into the rate equations for OSL, aiming to compare the influence of the thermal and optical probability on the electron trapping and detrapping mechanism. Lastly, as an example, we have used results obtained from MgB_4O_7:Ce,Li for supporting the presented discussion.

2. Methodologies

2.1. Experimental procedure

2.1.1. Materials synthesis and characterization

The synthesis of MgB_4O_7 doped with Ce and Li ions was carried out using the solid-state synthesis method. During the material production, the following analytical grade reagents were used: MgO (Alphatec, 99% purity), H_3BO_3 (Alphatec, 99.5% purity), CeO_2 (Alpha Aesar, 99.5% purity), and LiCl (Vetec, 99% purity).

Stoichiometric amounts of the reagents were homogenized in an agate mortar, placed in a porcelain crucible and annealed in a muffle furnace. For the annealing process, a heating rate of 10 °C/min and a maximum temperature of 900 °C, kept for 6 h, was used in a process that took place under an atmospheric air environment. The furnace was then turned off and the materials were submitted to a free and slowly cooling process until reaching room temperature (~25 °C). The produced material presented the following nominal concentrations for the dopants: MgB_4O_7:$Ce_{0.33wt\%}Li_{0.67wt\%}$. The chosen concentration for the Ce and Li was based on publications that discussed the optimal proportion with regards to luminescence emission [15,19], which indicated concentrations of MgB_4O_7:$Ce_{0.5wt\%}Li_{0.5wt\%}$ and MgB_4O_7:$Ce_{0.3mol\%}Li_{10mol\%}$ (the same as MgB_4O_7:$Ce_{0.24wt\%}Li_{0.39wt\%}$), respectively.

The structural and thermal properties, using techniques such as X-ray diffraction (XRD) and differential thermal analysis (DTA), as well as defect analysis of the material, using the atomistic simulation software GULP, were adequately reported in a previous study [20].

2.1.2. Thermoluminescence and optically stimulated Luminescence measurements

The irradiation procedure of the samples was carried out using a $^{90}Sr/^{90}Y$ beta radiation source from the RisØ TL/OSL reader, model DA-20, with a dose rate of 84.5 mGy s^{-1}. The exposure times using the quoted beta source were 20 s (1.69 Gy) and 180 s (15.21 Gy). The TL and OSL measurements were performed on the same reader.

The samples were examined in the form of pellets, which were approximately 5 mm in diameter, 2 mm thick, and weighed 40 mg. For the production of each pellet, the homogenized powder was uniaxially pressed at 1 ton force for 1 min. Right after irradiation, the entire batch was exposed to blue LED (peak emission at 470 nm; FWHM = 20 nm) for 0, 1, 3, 5, 10, and 20 s, with each light exposure conducted separately. TL measurements were taken from room temperature to 400 °C at a heating rate of 10 °C s^{-1} under a N_2 atmosphere. After each TL measurement the pellets were submitted to an annealing process, which involved a heating process up to 450 °C for 10 s in order to remove any residual signal. The annealing was performed in the reader itself. The entire procedure (beta irradiation - blue LED exposure - TL measurement - annealing process) was repeated for both 1.69 Gy and 15.21 Gy, which, as mentioned before, are related respectively to 20 s and 180 s of exposure.

For the optically stimulated luminescence analysis, after a 20 s beta irradiation the signal acquisition was performed using 40 s blue LED stimulation in the continuous wave method (CW-OSL). A Hoya U-340 filter, with transmission band between 290 nm and 390 nm, was used between the samples and the photomultiplier tube. The set of blue LEDs used to obtain the OSL signal was the same used in the light exposure before the TL analysis.

2.2. TL glow curve deconvolution

We used the 'tgcd' computational package in R to estimate the activation energies and frequency factor through the deconvolution of the experimental TL glow curve of the sample irradiated for 180 s with beta radiation [21]. The experimental TL glow curve was deconvoluted into five glow peaks using semi-analytical expressions of the one trap-one recombination (OTOR) model based on the Wright Omega function, assuming R-value = $A_n/A_m<1$ (where A_n and A_m are the electron recapture and recombination probabilities, respectively) [21–24]. Based on the OTOR model, an equation for the intensity of a single peak is obtained in terms of the Wright Omega function, as follows:

$$I(T) = I_M \, exp\left(-\frac{E}{KT}\frac{T_M - T}{T_M} \right) \frac{\omega(Z_M) + [\omega(Z_M)]^2}{\omega(Z) + [\omega(Z)]^2}$$

where:

$$Z_M = \frac{R}{1-R} - log\left(\frac{1-R}{R}\right) + E\frac{exp\left(\frac{E}{KT_M}\right)}{K(T_M)^2\left(1 - 1.05R^{1.26}\right)}F(T_M, E)$$

$$Z = \frac{R}{1-R} - log\left(\frac{1-R}{R}\right) + E\frac{exp\left(\frac{E}{KT_M}\right)}{K(T_M)^2\left(1 - 1.05R^{1.26}\right)}F(T, E)$$

being F (T, E) and F (T_M, E) given by Eqs:

$$F(T_M, E) = T_M \, exp\left(-\frac{E}{KT_M}\right) + \frac{E}{K}Ei\left(-\frac{E}{KT_M}\right)$$

$$F(T, E) = T_M \, exp\left(-\frac{E}{KT}\right) + \frac{E}{K}Ei\left(-\frac{E}{KT}\right)$$

I_M is the maximum TL intensity, T_M is temperature (K) at maximum TL intensity, k is Boltzmann constant (eV K^{-1}), E is activation energy (eV), T the temperature in K with constant heating rate K s^{-1}, ω and Ei are the wright Omega function and the exponential integral function, respectively.

We have also considered the Figure of Merit (FOM) and Squared Pearson Correlation (R^2) values as criteria for evaluating the goodness of fit of the experimental TL glow curve and the TL glow curve obtained from deconvolution [25,26].

2.3. Simulation of OSL decay curve in the presence of shallow traps

The simple theoretical framework used to explain the generation of the OSL signal in materials that contain electrons trapped also in shallow traps is shown in Fig. 1, which presents the main processes that may occur during the optical stimulation of the MgB_4O_7:Ce,Li at room temperature. We considered a simple model with five electron traps, in which trapped electrons (n_1, n_2, …, n_5) can be released by thermal and optical stimulation, and only one recombination centre. Re-trapping of released electrons and recombination (m) are competing processes. We chose a model with five traps to simulate the OSL decay curve because the deconvolution process revealed that the experimental TL glow curve of MgB_4O_7:Ce,Li was most accurately represented by the combination of five distinct peaks, as will be demonstrated in the forthcoming sections.

The thermal detrapping probability p_{Ti}, for trapped electrons to escape from traps to the conduction band, is given by Arrhenius law:

$$p_{Ti} = s_i\, e^{-\frac{E_i}{kT}} \quad (i = 1, 2, \ldots, 5) \tag{1}$$

where E_i (eV) is the activation energy of the electron traps (i = 1, 2, …,5), s_i (s^{-1}) is the frequency factor, k the Boltzmann constant, and T (K) the temperature. At room temperature, thermal energy is usually insufficient to release electrons in deep traps. However, we have introduced a thermal detrapping probability term for all traps for the sake of comparison with the optical detrapping probability. In this approach, the rate equations that govern the motion of charge carriers among the trapping levels, conduction band, and recombination centre, are given by Ref. [12]:

$$\frac{dn_i}{dt} = -n_i p_i - n_i p_{Ti} + n_c A_i (N_i - n_i) \;\; (i = 1, 2, \ldots, 5) \tag{2}$$

$$\frac{dn_c}{dt} = \sum_{i=1}^{5} [n_i p_i + n_i p_{Ti} - n_c A_i (N_i - n_i)] - n_c m A_m \tag{3}$$

$$\frac{dm}{dt} = -n_c m A_m \tag{4}$$

where N_i (cm^{-3}) and n_i (cm^{-3}) are the concentrations of total electron traps and filled electron traps, respectively. n_c (cm^{-3}) is the concentration of free carriers in the conduction band and m (cm^{-3}) is the concentration of the recombination centres. A_i ($cm^3\ s^{-1}$) and A_m ($cm^3\ s^{-1}$) are the capture probabilities of the electron traps and recombination centres, respectively. p_i is the detrapping probability due to an optical stimulus, which is determined by the product of the photoionization cross-section (σ, measured in cm^2) and the stimulated photon flux with wavelength λ (φ, measured in $cm^{-2}s^{-1}$). The photoionization cross-section is obtained by employing the Lima-Batista-Couto model [27] for localised states within the bandgap. By following the procedures outlined earlier in Ref. [27] and employing Fermi's golden rule, we achieve the following outcome:

$$\sigma = \frac{4\alpha\hbar^2 k^3}{m^{*2}\omega\omega_0}\sqrt{\frac{\pi\hbar}{m^*\omega_0}}\, exp\left\{ -\frac{\hbar}{m^*\omega_0}\left[k^2 + \left(\frac{\omega}{c}\right)^2\right]\right\} \times 4\pi\left(\frac{1}{\gamma(\omega)}\right)^3 [\gamma(\omega)cosh\,(\gamma(\omega)) - sinh\,(\gamma(\omega))] \tag{5}$$

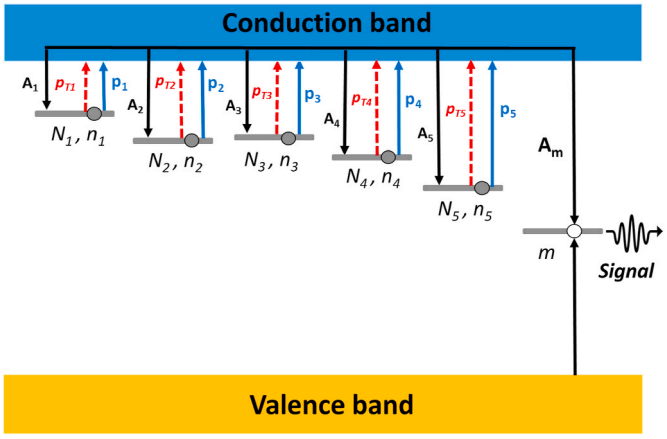

Fig. 1. Schematic representation of the trapping and re-trapping mechanism involved in the OSL signal of MgB_4O_7:Ce,Li. n_i is the concentration of trapped electrons into energy levels within the bandgap, m is the concentration of available recombination centres or trapped holes, and N_i is the total concentration of electron traps within the bandgap. A_i and A_m are the capture probabilities of the electron traps and recombination centres, respectively. p_i and p_{Ti} are the detrapping probabilities due to optical or thermal stimulation, respectively.

where $\gamma(\omega) = 2k\hbar\omega/\ m^*\omega_0 c$ represents an energy function, with ω and ω_0 denoting the angular frequencies of the incident electromagnetic radiation and the three-dimensional isotropic harmonic oscillator, respectively. The electron effective mass is denoted as m*, α is the fine structure constant, $\hbar$ is Planck's reduced constant, c represents the speed of light, and k is the wavevector of the electron. Eq. (5) represents the probability of a trapped electron being released to the conduction band, and after this potentially recombining with a hole at the recombination centre, emitting a photon with energy $\hbar\omega$.

The intensity of the OSL signal is proportional to the rate of recombination between holes and electrons, which can be written as:

$$I = n_c m A_m \tag{6}$$

Numerical methods implemented in Python have been used to obtain the solution of the presented set of differential equations.

3. Results and discussion

3.1. Analysis glow curve and estimate of the kinetic parameters

The TL glow curve obtained at a heating rate of 10 °C s^{-1} of the MgB_4O_7:$Ce_{0.33wt\%}$,$Li_{0.67wt\%}$ sample irradiated for 180 s with beta radiation was analysed using the 'tgcd' package in R, as proposed by Peng et al. [21]. In this study, the TL glow peaks were located by plotting the second-order derivative of the experimental TL curve. As depicted in Fig. 2, the TL glow curve of MgB_4O_7:$Ce_{0.33wt\%}$,$Li_{0.67wt\%}$ was well described by the combination of five peaks. The quality of fit of the experimental TL glow curve concerning the TL curve obtained in the deconvolution was evaluated by the FOM and R^2 values, considering

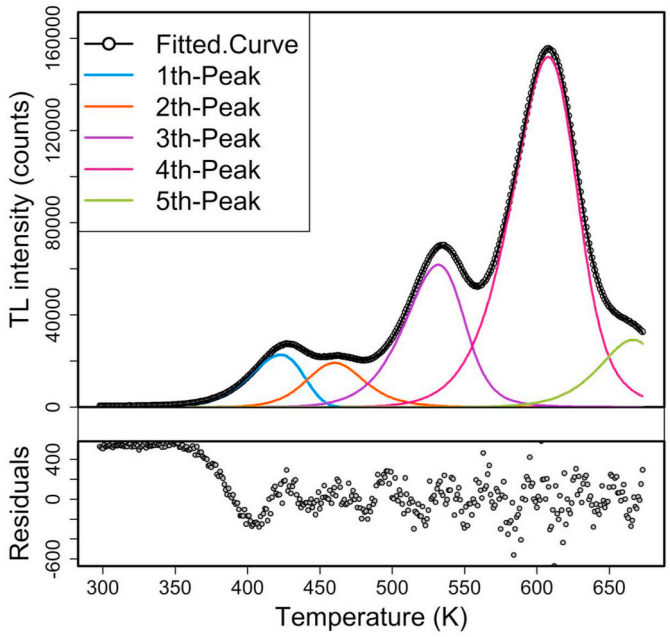

Fig. 2. Deconvoluted glow peaks for the TL glow curve of the MgB_4O_7:$Ce_{0.33wt\%}$,$Li_{0.67wt\%}$ sample using the OTOR model based on the Wright Omega function.

that FOM values in the range of 0–2.5% indicate a good fit, in the range of 2.5–3.5 the fit is reasonable, and >3.5 the fit is poor. Also, the closer the R^2 value is to 1, the better the curve fit [26]. We found values of FOM = 0.502 % and $R^2 = 0.999$, demonstrating an adequate fit of the TL glow curve in the deconvolution procedure. The activation energy and frequency factor values for each brightness peak were obtained from the expressions used in the 'tgcd' package. The activation energies for the five peaks are 0.8156 eV, 1.2567 eV, 1.2251 eV, 1.4677 eV, and 1.8795 eV, respectively, while the frequency factors are 2.80×10^9 s^{-1}, 3.34×10^{13} s^{-1}, 1.89×10^{11} s^{-1}, 6.25×10^{11} s^{-1}, and 7.99×10^{13} s^{-1}, respectively.

3.2. Time evolution of TL after optical stimulation

After exposing the material to the $^{90}Sr/^{90}Y$ source (dose rate of 84.5 mGy s^{-1}), several electrons become trapped in the bandgap of the material. Two different exposure durations were employed: 20 s and 180 s. In both cases, five distinct TL glow peaks, well-separated, have been observed around 423, 463, 532, 608 and 667 K. The peak around 423 K is associated with shallow traps, the peaks around 463 and 532 K with intermediate traps, while the remaining two peaks are attributed to deeper traps.

To get information about the electrons trapped at each specific trap, we analysed the changes on the TL glow curve after exposing the sample to optical stimulation from blue LEDs (emission peak at 470 nm). This procedure enables us to assess the electron concentration at each type of trap, as, under a linear heating rate, each TL glow peak correlates with the trapped electron population [28]. Consequently, an increase in the TL glow peak indicates an augmentation in the trapped electron concentration.

In view of analysing the behaviour of the TL glow curve obtained in different situations, we have employed different exposure times to optical stimulation, ranging from 0 to 20 s, in order to release electrons from the traps. Fig. 3 shows the TL glow curves recorded at t = 0 (without optical stimulation) and after optical stimulation durations of t = 1, 3, 5, 10, and 20 s. Relative changes in the intensity of the peaks were found, which should be connected to variations in the concentration of electrons trapped at each specific trap (N_1, N_2, …, N_5). The peak around 423 K, referring to the shallowest N_1 traps, increases around 10

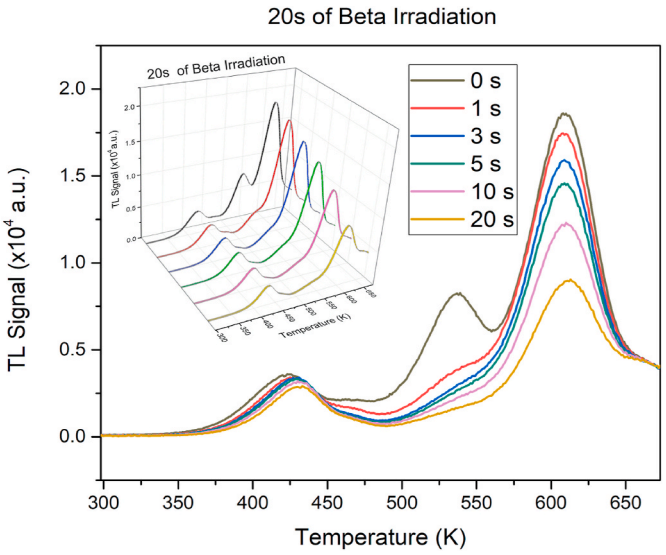

Fig. 3. TL glow curve of MgB_4O_7:Ce,Li before and after different durations (1, 3, 5, 10, and 20 s) of optical stimulation. The sample was exposed for 20 s to beta radiation.

% in the first second compared to the initial electron population. From 1 s of optical stimulation, the N_1 trapped electron concentration starts to slightly decrease, reaching almost 30 % of their population at 20 s. On the other hand, there is a significant decrease in the intermediate peaks around 463 and 532 K after the first second of optical stimulation. These observations clearly demonstrate that electrons trapped in intermediate traps (N_2 and N_3) are effectively released to the conduction band under blue light stimulation, with a very low probability of re-trapping. The population of electrons in N_2 and N_3 is practically emptied after 20 s of exposure to blue light. The peaks localised around 608 and 667 K, attributed to deeper N_4 and N_5 traps, present a reduction in their population of electrons due to optical stimulation, albeit at a slower decay rate than intermediate traps. After 20 s of optical stimulation, N_4 and N_5 traps maintain a higher electron concentration than the other traps. In this stage, the electron population in N_4 and N_5 traps decreased by almost 50 % compared to the initial concentration – comparing the areas

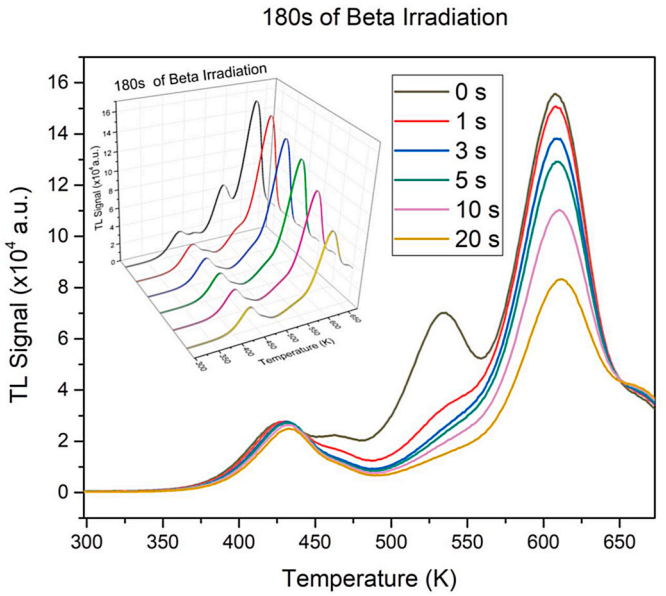

Fig. 4. TL glow curve of Li and Ce ions co-doped MgB_4O_7 after optical stimulation. The sample was exposed for 180 s to beta radiation.

below the TL glow curves.

Fig. 4 shows the TL glow curve of the sample after 180 s of radiation exposure. The TL signal is more intense compared to a 20 s exposure, as expected. The intermediate peaks around 463 and 532 K decrease by more than 50 % with just 1 s of optical stimulation, demonstrating that the trapping centres associated with these TL glow peaks only contribute to the OSL signal initially. However, the peak related to the shallow traps (423 K) again presents a rise in the first second and then starts to decrease. Indeed, after 180 s of radiation exposure, more electrons are trapped, resulting in a higher probability of charges released from the deep traps being captured in the shallow traps (if there is no saturation in the fill of the trap). Thus, the detrapping term has a greater influence on the kinetic of optically stimulated luminescence.

The results we found in the TL measurements suggest that the intermediate and deep traps are mainly responsible for the OSL signal. These results are in agreement with Yukihara et al. [15], who did not observe in MgB_4O_7:Ce,Li samples a decrease in the OSL signal for pre-heating temperatures up to ~423 K. Bossin et al. [29] found similar results for MgB_4O_7:Ce,Li; according to the authors, although shallower traps between 323 K–423 K do not contribute directly to the OSL signal, they could delay the luminescence emission by re-trapping charges or acting as competing centres.

3.3. OSL decay curve and trapping and detrapping parameters

The kinetic and trapping/detrapping mechanisms involved in the OSL decay curve of the MgB_4O_7:Ce,Li compound can be described by a rate law. By using a set of rate equations, as shown in section 2.3, it is possible to predict the magnitude of the rate parameters and how they can influence the OSL signal decay. In this case, the presented model considers five electron traps and one recombination centre in the face of the TL measurements. In a general sense, thermal and optical detrapping probabilities for shallow, intermediate and deep traps were considered, although the magnitude of p_T is too small for intermediate/deep traps.

The rate parameters are determined empirically through experimental results of the OSL decay curve and TL glow curve. Among the set of rate equations (Eq. 2 to 4), several adjustable parameters can be used to describe the charge carrier dynamics in this material. Out of these parameters, seven of them – n_1, n_2, n_3, n_4, n_5, n_c, and m represent the charge carrier population in each trap and/or conduction band – vary with the time while the other remain constant for any time.

TL measurements present in Figs. 3 and 4 enable us to assess the behaviour of the electron concentration in each trap using the set of rate equations. The thermal and optical detrapping parameters can be theoretically obtained by using the Arrhenius law (for p_{Ti}) and the Lima-Batista-Couto model (for p_i), respectively. p_{Ti} depends on the activation energy (E_i) and the frequency factor (s_i), while p_i depends on the photoionization cross-section and stimulated photon flux.

To get the detrapping probability rates (p_i) by optical stimulation, it is necessary to predict the photoionization cross-section (σ_i) of each trap. Additionally, apart from the activation energy, σ also depends on the electron effective mass (m*) and phonon frequency (ω_0). To the authors' knowledge, there is no information in the literature about m* of MgB_4O_7. As an approximation, we have used the value from the $Zn_4B_6O_{13}$ compound – borate material closest to MgB_4O_7 with available electron-effective mass data [30]. The phonon frequency (6.9×10^{14} rad/s) was obtained from the Raman spectrum for MgB_4O_7 [31], being calculated in the same way as presented in Ref. [32].

Fig. 5 presents the photoionization cross-section as a function of the electromagnetic radiation energy for each trap. The maximum probabilities of electron detrapping occur for the energies at 1.104 eV, 1.524 eV, 1.553 eV, 1.767 eV and 2.192 eV for each trap, respectively. By using the same wavelength ($\lambda = 470$ nm) employed to measure the OSL decay curve, we have obtained the following values for the photoionization cross-section of each trap: 7.6×10^{-19} cm^2 (Trap N_1), 3.5×10^{-18} cm^2 (Trap N_2), 3.1×10^{-18} cm^2 (Trap N_3), 6.9×10^{-18} cm^2 (Trap N_4), and 2.2×10^{-17} cm^2 (Trap N_5). Note that the N_1 shallow traps present the least electron detrapping probability to optical stimulation at 470 nm, as already demonstrated by the TL measurements after optical stimulation. On the other hand, the deeper traps (N_4 and N_5) exhibit the highest probability although the intermediate traps (N_2 and N_3) are quickly detrapped in a few seconds by optical stimulation, as shown in Figs. 3 and 4.

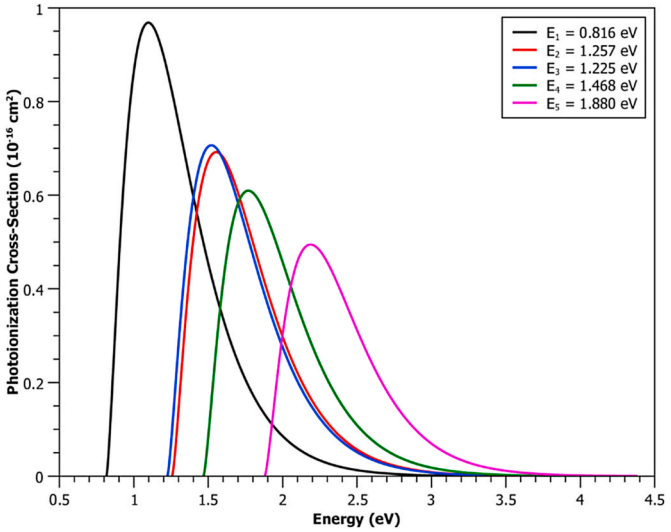

Fig. 5. Photoionization cross-section (cm^2) of the traps as a function of the electromagnetic radiation energy (eV) for Li and Ce ions co-doped MgB_4O_7. E_1, E_2, E_3, E_4 and E_5 are the activation energies of each trap.

In the face of values for the photoionization cross-section, we have calculated the electron detrapping probability due to an optical stimulus. With a stimulation wavelength of 470 nm and an experimental power density of 72 mW cm^{-2}, the calculated photon flux reached 1.7×10^{17} photons per second per cm^2. The energy of one photon is given by $E = h\nu$, $h = 6.63 \times 10^{34}$ W s^2 being Planck's constant and ν the linear frequency. For a blue-LED with wavelength $\lambda = 470$ nm, the energy produced by one photon is predicted to be 4.2×10^{-19} W s. Thus, the photon count per time and area units is given as follows: $\varphi = 1.7 \times 10^{17}$ cm^{-2} s^{-1} (0.072 W cm^{-2}/4.2×10^{-19} W s). The electron detrapping probabilities ($p = \sigma\varphi$) of each trap by optical stimulation are presented in Table 1. Note that electrons trapped in the shallowest traps (N_1) exhibit the lowest probability of being detrapped through optical stimulation, as indicated in Table 1.

By using the theoretical detrapping probability values, it becomes possible to empirically estimate the remaining rate parameters more reliably. The other kinetic parameters (A_i, N_i, n_i, and n_c) were acquired by fitting the experimental OSL decay curve for MgB_4O_7:Ce,Li through a set of rate equations (Eqs. (2)–(4)), as detailed in section 2.3. Table 1 presents all the kinetic parameters predicted in this study.

Fig. 6 shows that the chosen kinetic parameters in this study effectively adjusted the simulated OSL decay curve to match the experimental data from CW-OSL measurements. Notably, the probabilities of electron retrapping (A_i) were found to be higher for deeper and shallower traps in comparison to intermediate traps (as shown in Table 1). This observation aligns with expectations, considering that the experimental TL glow curves indicate that intermediate traps are almost emptied after 1 s of optical stimulation (as shown in Figs. 3 and 4). Some of the electrons released from intermediate traps migrate to shallower traps, as indicated by the increased peak intensity at 423 K in the TL glow curves after 1 s of optical stimulation. These findings provide a clearer understanding of the kinetics and trapping/detrapping mechanisms of the N_1 shallow traps, as observed in the TL glow curve after the optical stimulation. Instead, it acts to delay luminescence emission by re-trapping electrons from the conduction band.

Table 1
Kinetic parameters of both OSL and TL processes for the Li and Ce ions co-doped MgB_4O_7 compound. n_{i0} represents the trapped electron concentration at t = 0.

Level	N_i (cm^{-3})	n_{i0} (cm^{-3})	S_i (s^{-1})	p_{Ti} (s^{-1})	p_i (s^{-1})	A_i (cm^3s^{-1})	E_i (eV)
Trap ($i = 1$)	1.82×10^{14}	1.55×10^{14}	2.80×10^{9}	4.63×10^{-5}	0.130	3.10×10^{-10}	0.816
Trap ($i = 2$)	1.54×10^{14}	1.54×10^{14}	3.34×10^{13}	1.96×10^{-8}	0.598	1.00×10^{-13}	1.257
Trap ($i = 3$)	1.00×10^{15}	1.00×10^{15}	1.89×10^{11}	3.76×10^{-10}	0.538	5.80×10^{-13}	1.225
Trap ($i = 4$)	1.54×10^{16}	1.53×10^{16}	6.25×10^{11}	9.89×10^{-14}	1.181	1.40×10^{-9}	1.468
Trap ($i = 5$)	5.40×10^{14}	5.40×10^{14}	7.99×10^{13}	1.24×10^{-18}	3.771	1.10×10^{-9}	1.880
Recombination center ($i = m$)	–	–	–	–	–	1.80×10^{-11}	–

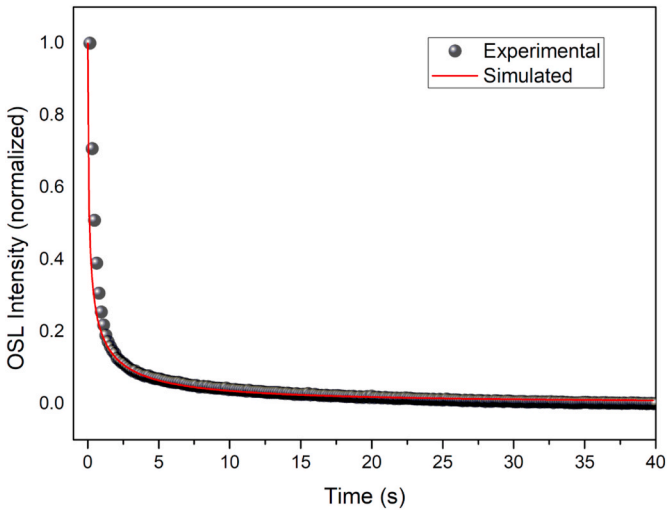

Fig. 6. Experimental (20 s of beta irradiation) and simulated OSL decay curve. The simulated decay curve was obtained by solving numerically the rate equations, and the rate parameters are presented in Table 1.

Moreover, we also assessed the time evolution of the trapped electron population in both N_1 and N_4 traps that emerge or are released due to blue-LED optical stimulation. Fig. 7a–b present the time evolution for the first 20 s of optical stimulation. The experimental points were acquired by measuring the peak areas at 423 K and 608 K in the TL glow curve (Fig. 3 with 20 s of beta irradiation) after successive optical stimulation, whereas the simulated data points were generated from the rate equations.

As shown in Fig. 7a and b, the simulated time evolution of the trapped electron population in N_1 and N_4 traps are very close to the experimental data. Additionally, n_1 increased around 10 % in the first second, before starting a downward trend. This behaviour is a consequence of the rapid emptying of intermediate traps and their low retrapping probability compared to deeper traps. Conversely, the intermediate traps exhibited a very low re-trapping (A_2/A_3), along with the highest detrapping probability when compared to the N_1 trap, providing strong evidence for the rapid emptying of the intermediate traps. Meanwhile, the trapped electron population in the N_4 traps has been steadily decreasing, in a way practically linear, since the onset of optical stimulation, with approximately 50 % of these traps being emptied within the initial 20 s. Thus, the shallow traps act to delay the luminescence emission by electron re-trapping from the conduction band released from intermediate traps, and not just as a TL trap. The decrease in the trapping electron population in the first 20 s is mainly due to the optical detrapping probability, which has a magnitude much greater than the thermal probability ($p_{Ti} \ll p_i$) as shown in Table 1.

3.4. Discussion

The presence of point defects within the material may result in traps of varying depths. The defect clustering created during the synthesis of the compound or by impurities is responsible for the formation process of these traps and recombination centres. For semiconductors and insulators, these traps are filled when the material is irradiated and electrons are prompted from the valence band to the conduction band and, subsequently, are captured by localised traps in the band gap. However, the existence of shallow traps poses a challenge when designing materials for applications in scintillation and ionising radiation dosimetry. This is problematic because shallow traps may have a deleterious effect by either reducing or delaying the luminescence emission, which is undesirable for these applications.

In some materials with shallow and deep traps, it is possible to observe differences in the trap emptying sequence between the TL and OSL processes. This difference is related to the participation of phonons in the electronic transition [33]. The local vibronic modes and the change between the ground and excited states are determined by the local crystal potential at the point defect that produces the trap. Therefore, electron-phonon coupling is specific to each trap and the difference between optical and thermal depths varies from trap to trap [33]. Occasionally, a trap identified as shallower in TL may have a greater optical depth than a deeper TL trap [33].

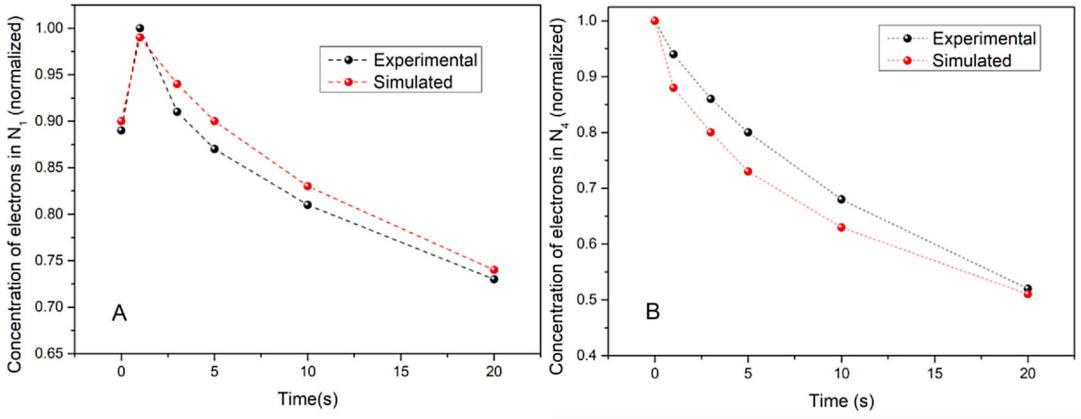

Fig. 7. Time evolution of the trapped electron population in both A) N_1 and B) N_4 traps that emerge or are released by optical stimulation.

Studies involving the MgB_4O_7 doped with rare earth and alkali metals have revealed the existence of shallow traps within the band gap, as supported by several works [15,29,34–38]. Specifically, in the case of co-doping with Li and Ce ions, the TL glow curve exhibits five distinct peaks, with one of them attributable to the presence of shallow traps. TL measurements subsequent to the optical stimulation show a quick emptying of intermediate traps (N_2 and N_3) and a slight increase of the N_1 shallow traps in the first second, whereas the N_4 deeper traps start a decay tendency practically linear since the first second.

The predictions of the thermal and optical detrapping probabilities using Arrhenius law and the Batista-Lima-Couto model, respectively, revealed that N_1 shallow traps exhibit a higher thermal detrapping probability (p_{T1}) compared to other traps, although with a magnitude lower than the optical detrapping probability (p_1) – $p_{T1}<p_1$. In this case, p_{T1} is sufficient for electron detrapping from shallow traps before initiating the optical stimulus, and provoking a short-term fading of the OSL decay curve as shown by Yukihara et al. [15]. Furthermore, this electron detrapping at room temperature leads to an electron population different from zero in the conduction band for $t = 0$ s. Using this boundary condition is essential to adjust the OSL decay curve. Thus, we considered by rate law that $n_c/n_1 = p_{T1}$ at $t = 0$ s (without optical stimulation).

Conversely, when we assessed the optical detrapping probabilities obtained by the Batista-Lima-Couto model, it became evident that N_1 shallow traps exhibit a notably lower magnitude compared to intermediate and deeper traps for an optical stimulation wavelength at 470 nm. This finding contrasts with the suggestion of Yukihara et al. [15], associating them with the fastest OSL components as a consequence of the high photoionization cross-section. Also, the re-trapping rate (A_1) associated with N_1 shallow traps has a higher magnitude than intermediate traps leading to a delay in the luminescence emission.

Among all traps, N_1 shallow traps have the lowest decay rate of trapped electrons, decreasing less than 30 % of the trapped electron population between 1 and 20 s of optical stimulation, because of high re-trapping and low photoionization cross-section. Meanwhile, intermediate traps are practically emptied in this period and N_4 traps decrease by almost 50 % of the initial value. Our results agree with the results reported by Bossin et al. [29] about TL measurements recorded at a heating rate of 1 °C s^{-1} in MgB_4O_7: $Ce_{0.3mol\%}$, $Li_{10mol\%}$ after exposure to blue LED (470 nm) for durations ranging from 1 s to 120 s. There, the mean peak associated with the deeper traps decrease in the same proportion as our TL measurements. For instance, in both the TL results presented by us and those by Bossin et al. [29], there is a reduction of approximately 30 % in the TL peak associated with the deepest trap (N_4) after 10 s of optical stimulation with blue light. Also, in both studies, it is noticeable that the intermediate peak of the TL measurement is almost completely extinguished after only 10 s of optical stimulus. However, unlike our findings, in the TL measurements conducted by Bossin et al. [29], the peak corresponding to the shallower trap appears to increase during a 10 s stimulus and remains constant for up to 120 s.

This difference in this behaviour may be associated to the fact that MgB_4O_7:$Ce_{0.3mol\%}$,$Li_{10mol\%}$ has shallow traps that are either less populated or have a higher probability of re-trapping, in comparison to the material produced by us (MgB_4O_7:$Ce_{0.33wt\%}$,$Li_{0.67wt\%}$). According to Yukihara et al. [39], a higher number of empty traps (N–n) corresponds to a proportionally greater re-trapping probability, leading to a delay in the recombination process. It is noteworthy that the presence of Li in the material likely contributes to the existence of these shallow traps. In our prior work, we did not observe a TL peak at approximately 423 K in samples doped solely with Ce [20].

For MgB_4O_7:Ce, the luminesce signal may be associated with two probable defect clustering's ($Ce^{\bullet}_{Mg}Mg'_B$ or $Ce^{\bullet\bullet\bullet}_{i}Mg'_BO''_i$), while for MgB_4O_7:Ce,Li, it may be associated with the $2Li\ '_{Mg}Ce^{\bullet\bullet\bullet}_{i}Mg'_B$ defect clustering. In all cases, the Mg'_B defect is present in the host matrix. When comparing both possibilities where Ce ions occupy an interstitial position, the main distinguishing factor is the presence of a Li substitutional defect into Mg site [20].

Another crucial aspect is the origin of these point defects. In a prior study, we suggested that the mechanism of defect formation originates from the decomposition process of magnesium precursors during synthesis [20,40]. Guckan et al. [41] developed a luminescence properties study of Li and Ce ions co-doped MgO, using a solid-state reaction synthesis, and obtained a TL glow curve exhibiting a similar behaviour to what is presented here. The TL glow curve of MgO:Li,Ce features five peaks in the temperature range of 353–723 K, reinforcing the connection between defect clustering and luminescence centres having a common origin for these phenomena in both materials.

4. Conclusion

In summary, we have used Thermoluminescence (TL) and Optically Stimulated Luminescence (OSL) measurements associated to kinetic models to shed light on the intricate dynamics of charge carriers within materials containing multiple trap and a single recombination centre, with a specific focus on Li and Ce co-doped MgB_4O_7. The new findings exhibited here are:

- The electron populations trapped in shallower traps exhibited a slower decay rate under optical stimulation compared to intermediate and deep traps;
- The delay in luminescence emission is attributed to charge re-trapping or competition with other centres due to the low photoionization cross-section and high re-trapping rate of the shallower traps;
- The electron population in the conduction band is different of zero at $t = 0$ (before optical stimulation) due to the magnitude of the thermal probability;
- In the first second of optical stimulation, the intermediate traps are the main responsible for the OSL signal because of the high photoionization-cross section and very low re-trapping rate;
- The trapped electron population in the N_4 deeper traps decreases practically linearly during the time stage, reaching almost 50 % of the initial population in the first 20 s.

Lastly, this study has provided valuable insights to understand the dynamics of charge carriers in systems containing multiple traps, offering new elements for improving the performance of materials in scintillation and dosimetry applications. By understanding the behaviour of shallow traps and their interactions with charge carriers, it is possible to design materials with enhanced characteristics and functionality for specific applications. Thus, these findings pave the way for future advancements in the development of materials for several applications.

CRediT authorship contribution statement

Adelmo S. Souza: Writing – original draft, Visualization, Methodology, Investigation, Formal analysis, Data curation, Conceptualization. **Jorge L.O. Santos:** Writing – review & editing, Writing – original draft, Validation, Methodology, Formal analysis, Data curation, Conceptualization. **Vinicius Coelho:** Validation, Methodology, Investigation. **Antonio O. de Souza:** Validation, Methodology, Investigation. **João V. B. Valença:** Writing – original draft, Validation, Methodology, Investigation. **Iury S. Silveira:** Validation, Methodology, Investigation. **Linda V.E. Caldas:** Visualization, Validation, Investigation. **Heveson Lima:** Writing – review & editing, Writing – original draft, Visualization, Validation, Supervision, Project administration, Investigation, Formal analysis, Data curation, Conceptualization.

Declaration of competing interest

The authors declare that they have no known competing financial

interests or personal relationships that could have appeared to influence the work reported in this paper.

Data availability

Data will be made available on request.

Acknowledgment

The authors acknowledge the CNPq Projects (310586/2021-6, 404784/2021-6 and 305142/2021-6), CAPES, FINEP, and FAPESB/BA – Brazilian Funding Agencies – for financial support.

References

[1] L. Yuan, Y. Jin, Y. Su, H. Wu, Y. Hu, S. Yang, Optically stimulated luminescence phosphors: principles, applications, and prospects, Laser Photon. Rev. 14 (2020) 2000123, https://doi.org/10.1002/LPOR.202000123.
[2] E.G. Yukihara, G. Mardirossian, M. Mirzasadeghi, S. Guduru, S. Ahmad, Evaluation of optically stimulated luminescence (OSL) dosimeters for passive dosimetry of high-energy photon and electron beams in radiotherapy, Med. Phys. 35 (2008) 260–269, https://doi.org/10.1118/1.2816106.
[3] E.J. Guidelli, A.P. Ramos, O. Baffa, Silver nanoparticle films for metal enhanced luminescence: toward development of plasmonic radiation detectors for medical applications, Sensor. Actuator. B Chem. 224 (2016) 248–255, https://doi.org/10.1016/J.SNB.2015.10.024.
[4] C. Wouter, V. Dirk, L. Paul, D. Tom, A reusable OSL-film for 2D radiotherapy dosimetry, Phys. Med. Biol. 62 (2017) 8441, https://doi.org/10.1088/1361-6560/AA8DE6.
[5] K. Takegami, H. Hayashi, H. Okino, N. Kimoto, I. Maehata, Y. Kanazawa, T. Okazaki, T. Hashizume, I. Kobayashi, Estimation of identification limit for a small-type OSL dosimeter on the medical images by measurement of X-ray spectra, Radiol. Phys. Technol. 9 (2016) 286–292, https://doi.org/10.1007/S12194-016-0362-5/METRICS.
[6] E. Martín Rodríguez, G. López-Peña, E. Montes, G. Lifante, J. García Solé, D. Jaque, L.A. Diaz-Torres, P. Salas, Persistent luminescence nanothermometers, Appl. Phys. Lett. 111 (2017), https://doi.org/10.1063/1.4990873/35063.
[7] A. Sato, Y. Takahashi, N. Terakado, T. Miyazaki, N. Onoue, T. Shinozaki, T. Fujiwara, Potential of afterglow zirconia as a sensitive biological temperature probe, Ceram. Int. 48 (2022) 25587–25591, https://doi.org/10.1016/J.CERAMINT.2022.05.238.
[8] E.G. Yukihara, S.W.S. McKeever, M.S. Akselrod, State of art: optically stimulated luminescence dosimetry – frontiers of future research, Radiat. Meas. 71 (2014) 15–24, https://doi.org/10.1016/J.RADMEAS.2014.03.023.
[9] A. Vedda, M. Fasoli, Tunneling recombinations in scintillators, phosphors, and dosimeters, Radiat. Meas. 118 (2018) 86–97, https://doi.org/10.1016/J.RADMEAS.2018.08.003.
[10] A.S. Altowyan, Ü.H. Kaynar, K. Bulcar, M. Oglakci, Z.G. Portakal-Uçar, J. Hakami, M. Topaksu, N. Can, Unusual heating rates, dose responses and kinetic parameters detected on thermoluminescence from YAl3(BO3)4:Sm3+ phosphors, Ceram. Int. 49 (2023) 33291–33304, https://doi.org/10.1016/J.CERAMINT.2023.08.038.
[11] S. Atasöz, M. Topaksu, G. Souadi, N. Can, Anomalous heating rate dependence and analyses of thermoluminescence glow curves in Gd doped ZnB2O4 phosphors, J. Lumin. 246 (2022) 118838, https://doi.org/10.1016/J.JLUMIN.2022.118838.
[12] G. Denis, M.S. Akselrod, E.G. Yukihara, Influence of shallow traps on time-resolved optically stimulated luminescence measurements of Al2O3:C,Mg, J. Appl. Phys. 109 (2011) 104906, https://doi.org/10.1063/1.3584791/985248.
[13] O.V. Pakari, J.B. Christensen, E.G. Yukihara, L. Bossin, The effect of shallow and deep traps on the determination of thermal quenching using pulsed optically stimulated luminescence: the case of Al2O3:C, J. Lumin. 248 (2022) 118982, https://doi.org/10.1016/J.JLUMIN.2022.118982.
[14] Y. Kitagawa, E.G. Yukihara, S. Tanabe, Development of Ce3+ and Li+ co-doped magnesium borate glass ceramics for optically stimulated luminescence dosimetry, J. Lumin. 232 (2021) 117847, https://doi.org/10.1016/J.JLUMIN.2020.117847.
[15] E.G. Yukihara, B.A. Doull, T. Gustafson, L.C. Oliveira, K. Kurt, E.D. Milliken, Optically stimulated luminescence of MgB_4O_7:Ce,Li for gamma and neutron dosimetry, J. Lumin. 183 (2017) 525–532, https://doi.org/10.1016/j.jlumin.2016.12.001.
[16] R. Chen, P.L. Leung, Nonlinear dose dependence and dose-rate dependence of optically stimulated luminescence and thermoluminescence, Radiat. Meas. 33 (2001) 475–481, https://doi.org/10.1016/S1350-4487(01)00034-8.
[17] M. Jain, R. Kumar, M. Kook, A novel coupled RPL/OSL system to understand the dynamics of the metastable states, Sci. Rep. 10 (2020) 15565, https://doi.org/10.1038/s41598-020-72434-4.
[18] J. Yin, G.H. Ahmed, O.M. Bakr, J.L. Brédas, O.F. Mohammed, Unlocking the effect of trivalent metal doping in all-inorganic CsPbBr3 perovskite, ACS Energy Lett. 4 (2019) 789–795, https://doi.org/10.1021/ACSENERGYLETT.9B00209/SUPPL_FILE/NZ9B00209_SI_001.PDF.
[19] L.F. Souza, A.L.F. Novais, P.L. Antonio, L.V.E. Caldas, D.N. Souza, Luminescent properties of MgB4O7:Ce,Li to be applied in radiation dosimetry, Radiat. Phys. Chem. 164 (2019) 108353, https://doi.org/10.1016/J.RADPHYSCHEM.2019.108353.
[20] J.V.B. Batista, H. Trombini, A. Otsuka, I.S. Silveira, L.V.E. Caldas, A.O. de Souza, A. S. Souza, J.L.O. Santos, V. Coelho, H. Lima, Unlocking the effect of Li and Ce ions on the thermoluminescence and optically stimulated luminescence signals of the MgB4O7 compound, Dalton Trans. 52 (2023) 6407–6419, https://doi.org/10.1039/D3DT00485F.
[21] J. Peng, Z.B. Dong, F.Q. Han, tgcd: an R package for analyzing thermoluminescence glow curves, SoftwareX 5 (2016) 112–120, https://doi.org/10.1016/j.softx.2016.06.001.
[22] L. Lovedy Singh, R.K. Gartia, Theoretical derivation of a simplified form of the OTOR/GOT differential equation, Radiat. Meas. 59 (2013) 160–164, https://doi.org/10.1016/J.RADMEAS.2013.04.022.
[23] L. Lovedy Singh, R.K. Gartia, Glow-curve deconvolution of thermoluminescence curves in the simplified OTOR equation using the Hybrid Genetic Algorithm, Nucl. Instrum. Methods Phys. Res. B 319 (2014) 39–43, https://doi.org/10.1016/J.NIMB.2013.10.029.
[24] L.L. Singh, R.K. Gartia, Derivation of a simplified OSL OTOR equation using Wright Omega function and its application, Nucl. Instrum. Methods Phys. Res. B 346 (2015) 45–52, https://doi.org/10.1016/J.NIMB.2015.01.038.
[25] G. Kitis, G.S. Polymeris, I.K. Sfampa, M. Prokic, N. Meriç, V. Pagonis, Prompt isothermal decay of thermoluminescence in MgB4O7:Dy,Na and LiB4O7:Cu, in dosimeters, Radiat. Meas. 84 (2016) 15–25, https://doi.org/10.1016/J.RADMEAS.2015.11.002.
[26] R.K. Gartia, L.L. Singh, Evaluation of trapping parameter of quartz by deconvolution of the glow curves, Radiat. Meas. 46 (2011) 664–668, https://doi.org/10.1016/J.RADMEAS.2011.06.036.
[27] H. Lima, J.V. Batista, M.A. Couto Dos Santos, Photoionization cross-section of isotropic defects or impurity centers in isolators, Europhys. Lett. 115 (2016) 33002, https://doi.org/10.1209/0295-5075/115/33002.
[28] A.M. Sadek, H.M. Eissa, A.M. Basha, G. Kitis, Resolving the limitation of the peak fitting and peak shape methods in the determination of the activation energy of thermoluminescence glow peaks, J. Lumin. 146 (2014) 418–423, https://doi.org/10.1016/J.JLUMIN.2013.10.031.
[29] L. Bossin, I. Plokhikh, J.B. Christensen, D.J. Gawryluk, Y. Kitagawa, P. Leblans, S. Tanabe, D. Vandenbroucke, E.G. Yukihara, Addressing current challenges in OSL dosimetry using MgB4O7:Ce,Li: state of the art, limitations and avenues of research, Materials 16 (2023) 3051, https://doi.org/10.3390/MA16083051/S1.
[30] Y. Li, Y. Diao, X. Wang, X. Tian, Y. Hu, B. Zhang, D. Yang, Zn4B6O13: efficient borate photocatalyst with fast carrier separation for photodegradation of tetracycline, Inorg. Chem. 59 (2020) 13136–13143, https://doi.org/10.1021/ACS.INORGCHEM.0C01425/SUPPL_FILE/IC0C01425_SI_001.PDF.
[31] E. Ekdal, J. Garcia Guinea, Y. Karabulut, A. Canimoglu, C. Harmansah, A. Jorge, T. Karali, N. Can, Characterisation and luminescence studies of Tm and Na doped magnesium borate phosphors, Appl. Radiat. Isot. 103 (2015) 93–99, https://doi.org/10.1016/J.APRADISO.2015.05.023.
[32] A. Togo, I. Tanaka, First principles phonon calculations in materials science, Scripta Mater. 108 (2015) 1–5, https://doi.org/10.1016/J.SCRIPTAMAT.2015.07.021.
[33] A. Chruścińska, P. Palczewski, OSL characteristics: theory and experiments, Radiat. Protect. Dosim. 192 (2020) 266–293, https://doi.org/10.1093/RPD/NCAA205.
[34] E.C. Karsu, M. Gökçe, A. Ege, T. Karali, N. Can, M. Prokic, Kinetic characterization of MgB4O7:Dy,Na thermoluminescent phosphor, J. Phys. D Appl. Phys. 39 (2006) 1485, https://doi.org/10.1088/0022-3727/39/8/005.
[35] C. Furetta, G. Kitis, P.S. Weng, T.C. Chu, Thermoluminescence characteristics of MgB4O7:Dy,Na, Nucl. Instrum. Methods Phys. Res. 420 (1999) 441–445, https://doi.org/10.1016/S0168-9002(98)01198-X.
[36] A. Ozdemir, V. Guckan, V. Altunal, K. Kurt, Z. Yegingil, Thermoluminescence in MgB4O7:Pr,Dy dosimetry powder synthesized by solution combustion synthesis method, J. Lumin. 230 (2021) 117761, https://doi.org/10.1016/J.JLUMIN.2020.117761.
[37] V. Pagonis, N. Brown, G.S. Polymeris, G. Kitis, Comprehensive analysis of thermoluminescence signals in MgB4O7:Dy,Na dosimeter, J. Lumin. 213 (2019) 334–342, https://doi.org/10.1016/J.JLUMIN.2019.05.044.
[38] P.R. González, O. Ávila, L. Escobar-Alarcón, D. Mendoza-Anaya, Luminescence and kinetics parameters of high sensitivity MgB4O7 phosphor co-doped with Tm and Dy, Appl. Radiat. Isot. 175 (2021) 109811, https://doi.org/10.1016/J.APRADISO.2021.109811.
[39] E. Gardenali Yukihara, TL and OSL as research tools in luminescence: possibilities and limitations, Ceram. Int. 49 (2023) 24356–24369, https://doi.org/10.1016/J.CERAMINT.2022.10.199.
[40] R. Contassot, J. Batista, A. Otsuka, A. Souza, E. Ferraz, A.S. Souza, J.L.O. Santos, V. Coelho, H. Lima, Elucidating the effect of intrinsic defects on the dosimetric properties of the MgB4O7 compound: an atomistic simulation approach, New J. Chem. 46 (2022) 6403–6413, https://doi.org/10.1039/D1NJ06080E.
[41] V. Guckan, S.W. Bokhari, V. Altunal, A. Ozdemir, W. Gao, Z. Yegingil, Luminescence of Ce3+ and Li+ co-doped MgO synthesized using solid-state reaction method, Nucl. Instrum. Methods Phys. Res. B 503 (2021) 53–61, https://doi.org/10.1016/J.NIMB.2021.07.012.